The Corrosion of Various Materials under Chloride Deposits at 623-723K in Pure Oxygen

YS. Li, M. Al-Omary [o], Y. Niu* and K. Zhang

State Key Labolatory for Corrosion & Protection, Institute of Metal Research (South Campus) Wencui Road 62, Shenyang 110016,China
[o] Dept. of Basic Sciences, University of Sharjah, P.O. Box 28267 Sharjah, United Arab Emirates

(Received December 10, 2001: final form February 6, 2002)

ABSTRACT

Corrosion problems in waste incinerators or in other advanced combustion power generation systems are usually rather serious due to the deposition of ashes composed of heavy and alkali metal chlorides or sulfates of metals such as Zn, K, Pb etc. This paper presents the individual and combined effects of $ZnCl_2$ and KCl on the corrosion behavior of some heat-resistant steels, the M38G Ni-based alloy, 2205 duplex steel and several other Fe-based alloys as well as pure metals were examined at 623K and 723K in pure oxygen. All the materials tested suffered from accelerated corrosion due to the formation of non-protective porous oxide scales and in many cases from local attack in the alloy matrix induced by chlorine. The Cr addition to the alloys can hardly provide sufficient corrosion resistance against such environments as a result of the bad adherence of Cr_2O_3 to the alloy matrix. This detrimental effect is discussed on the basis of thermodynamic considerations.

Key words: chloride deposits, corrosion, alloys, waste incineration

INTRODUCTION

Incineration has been adopted as an effective and hygienic method for the disposal of the ever-increasing voluminous industrial and municipal solid waste in many countries /1,2/. For example, in Western Europe only, about 600 plants are presently in operation and their number is still increasing. Even though this is a comparatively new business in China, more and more large-scale waste incineration factories are being built in many big cities at present /1/. This is especially encouraged because the average heat of combustion of municipal waste in China has increased greatly and may reach now 4180 KJ/kg or more, which will be very suitable for incineration disposal. In most cases, the corrosion problems in incineration environments are very severe due to the complex reactions between the combustion gases containing chlorine and sulfur and the salt deposits mostly composed of chlorides and sulfates, so that metallic materials usually undergo aggressive corrosion and degrade completely in times much shorter than the designed life. For example, the super-heater tube materials used in the waste incinerator of Shenzhen degraded seriously in less than three months after service, and had to be changed totally. However, the

* Corresponding author. Fax: +86-24-23894149.
E-mail: yniu@icpm.syb.ac.cn (Y Niu)

individual corrosion effects of the heavy metal (Sn, Pb, Zn) or alkali metal (K, Na) chlorides, which are actually the major components in deposits from waste incinerators, have not been examined thoroughly /3-5/. In fact, up to now the attention has been mostly focused on the corrosion mechanisms caused by sulfate salts or by gaseous chlorides. In this study, the corrosion behavior of several Fe-based alloys, of a commercial Ni-based alloy as well as that of pure Fe and Cr, is investigated in the presence of $ZnCl_2$/KCL deposits at 723K in the absence of Cl compounds in the gas phase.

EXPERIMENTAL MATERIALS AND PROCEDURES

The chemical composition of the materials employed in this study is shown in Table 1. In particular, the heat-resistant HP steel contains two phases, i.e. a γ matrix plus particles of the Cr_7C_3 carbide. The duplex stainless steel 2205 has an average Cr content of 22 wt.% and is composed of a mixture of a Cr-rich ferritic α phase (with 26 wt.% Cr) and an austenitic γ phase (with 20 wt.% Cr). All the materials were machined into specimens with dimensions of about 10 x 15 x 1.5 mm, then ground to 600 SiC paper and subsequently cleaned with acetone. After being preheated, the samples were coated either with pure KCl or pure $ZnCl_2$ (1-2mg/cm^2) or with a $ZnCl_2$-KCl mixture (55: 45, molar ratio) (3-4mg/cm^2), homogeneously distributed on the sample surfaces.

The experiments were carried out in 0.1MPa of a pure oxygen with a flow velocity of 80 ml/s controlled by a capillary flowmeter, using a horizontal furnace equipped with a quartz working tube. Each of the salt-coated samples was hung in an alumina crucible with a platinum wire, after which the crucibles were placed into the pre-heated horizontal furnace. The corrosion kinetics were monitored regularly by moving out the samples and putting them back after measuring their weight. Some typical samples were also corroded by complete immersion in the molten salts for comparison purposes.

After corrosion, metallurgical cross-sections were prepared by grinding the samples in kerosene in order to prevent the dissolution of the chlorides from the scale. The morphological and composition analysis were carried out using Scanning Electron Microscopy (SEM), Energy Dispersive X-Ray Spectroscopy (EDX) and X-Ray Diffraction (XRD).

Table 1
Nominal chemical composition of the materials tested (in wt.%)

	Fe	Cr	Ni	Other
Fe	bal	-	-	-
Cr	-	bal	-	-
Ni	-	-	bal	-
Carbon steel	bal	-	-	0.45 Mn; 0.2 C
P91	bal.	8.60	0.26	0.93 Mo; 0.41 Mn
2205	bal	22.20	5.80	1.56 Mn; 3.05 Mo
SS310	bal	23.4	18.2	8.69 Mo; 1.70 Si
HP	bal.	25.60	35.08	C 0.40, Si 1.06, Mn 0.88
M38G	-	16.34	bal	4.01Al; 3.38Co; 3.81Ti; 2.70W; 1.77Mo; 1.75Ta; 0.76Nb, 0.16C
FeAl	bal	-	-	26.00 Al

RESULTS

Corrosion kinetics

Figure 1 shows the kinetic curves for the corrosion of pure Fe and three Fe-based alloys beneath pure $ZnCl_2$ deposit. The mass changes are very irregular, and in particular a mass loss was always present during the initial corrosion stage, which later transformed into a nearly constant mass value for Fe, P91 and HP, while the carbon steel presented a second stage of fast mass gain. An important reason for the kinetic behavior observed is the strong evaporation of $ZnCl_2$, which prevails over the mass increase due to the oxidant pickup during the initial period, even though an accelerated corrosion is present for the whole duration of the tests. The carbon steel corrodes much more rapidly than the other materials, producing a net mass gain after a short initial stage.

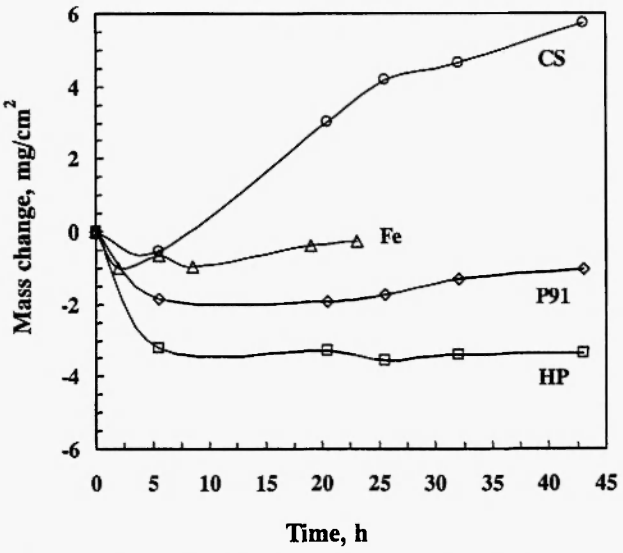

Fig. 1: Corrosion kinetics of pure Fe and three Fe-based alloys beneath a $ZnCl_2$ deposit at 723K in 0.1MPa O_2 for times up to 43 hrs.

Figure 2 shows the kinetic curves for the corrosion of the materials listed in Table I beneath $ZnCl_2$-KCl deposits at 723K. For all the materials examined the attack under mixed $ZnCl_2$-KCl deposits was heavier. The results for pure Cr were not included in the plot since the corrosion products spalled off very extensively during the initial corrosion stage (less than 1 h). The corrosion rates were all markedly enhanced with respect to pure oxidation during an initial stage, which was then followed by a stage of very slow corrosion rate. Among the various materials, pure Fe, the carbon steel and the Cr-rich Fe-based alloys (2205, SS310) have the largest mass gains. An increase of the Cr content of the Fe-based alloys results in larger corrosion rates under KCl-$ZnCl_2$ deposits. The alloys rich in nickel (M38G and HP) as well as FeAl have relatively low corrosion rates.

The kinetic curves of the carbon steel (CS), a medium Cr steel (P91) and a high chromium nickel steel

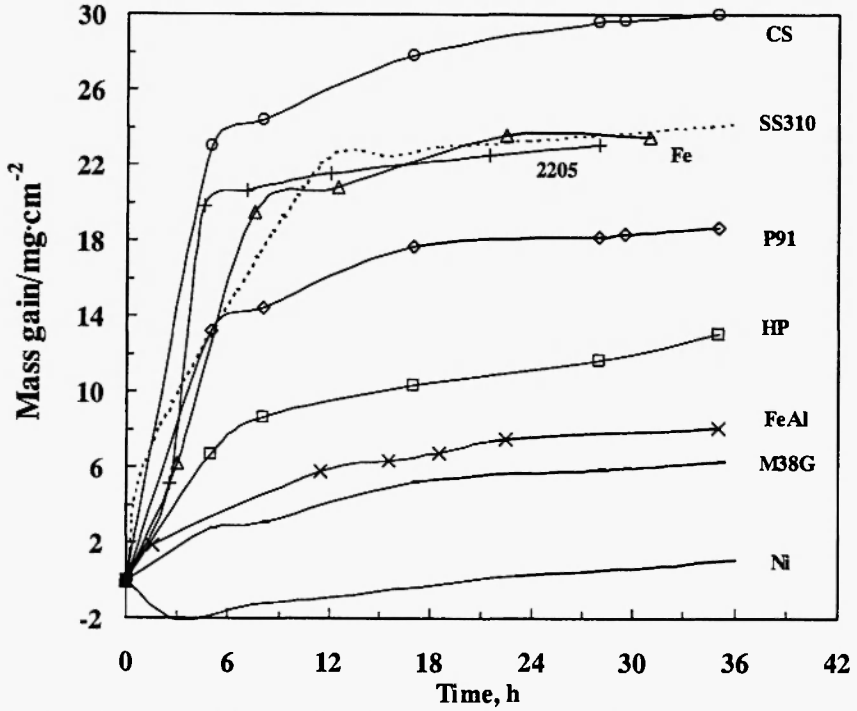

Fig. 2: Corrosion kinetics of the materials examined beneath a $ZnCl_2$-KCl deposit at 723K in 0.1MPa O_2 for times up to 36 hrs.

(HP) corroded under mixed KCl-$ZnCl_2$ deposits in pure oxygen at both 623K and 723K (Fig. 3) show a large effect of temperature on the corrosion rate of all these materials.

Scale structure and composition

The four materials corroded beneath $ZnCl_2$ deposit at 723K formed thick and irregular external scales, rather porous and partly cracked (Fig. 4). For CS (Fig.

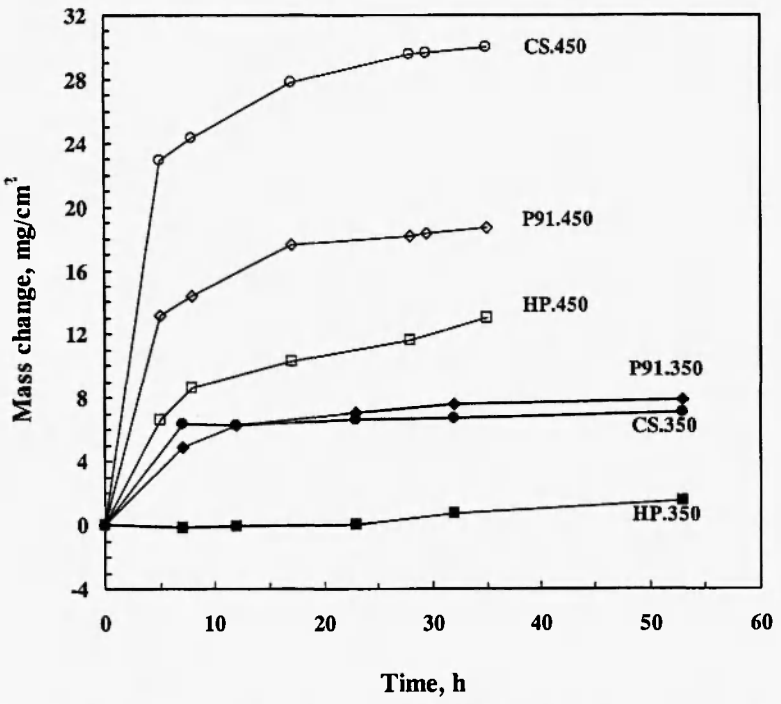

Fig. 3: Corrosion kinetics of three Fe-based alloys beneath a $ZnCl_2$-KCl deposit at 623K and 723k in 0.1MPa O_2 for times up to 36 hrs.

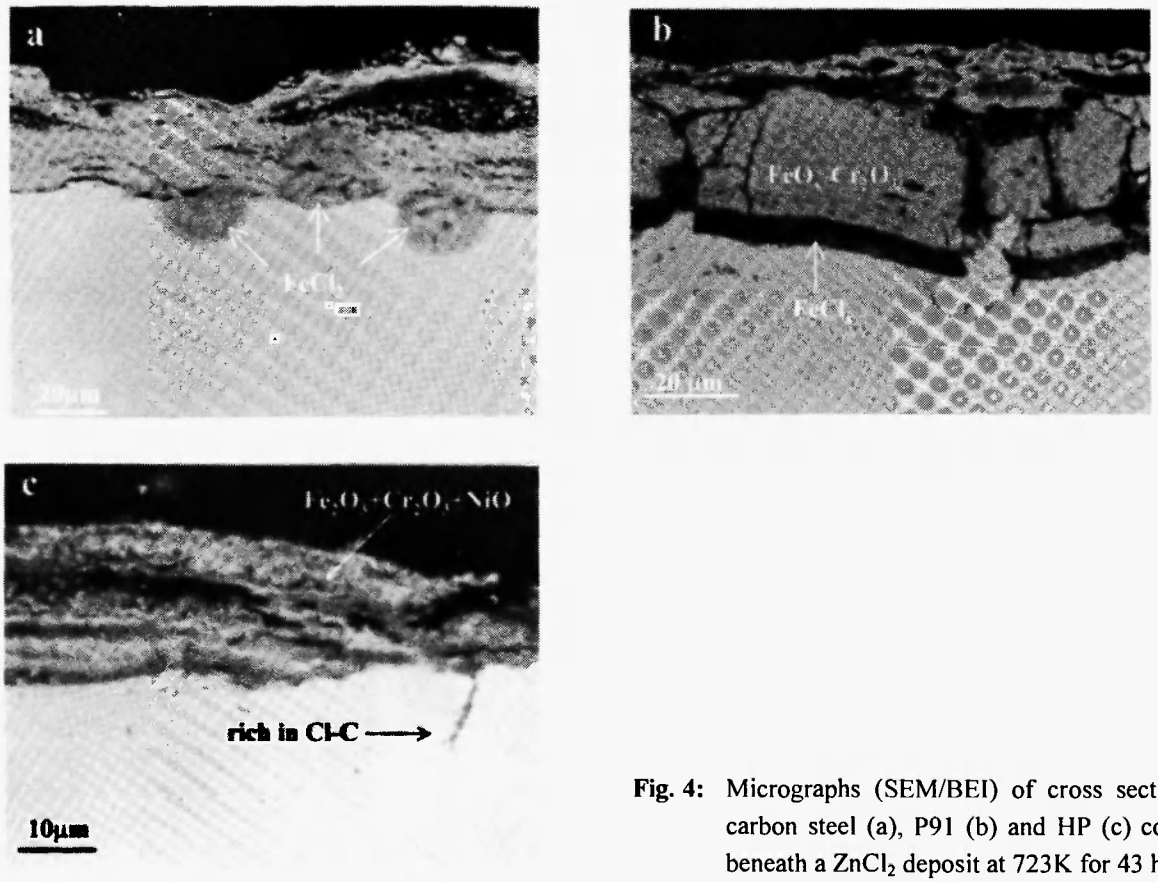

Fig. 4: Micrographs (SEM/BEI) of cross sections of carbon steel (a), P91 (b) and HP (c) corroded beneath a $ZnCl_2$ deposit at 723K for 43 hrs.

4a) and P91 (Fig. 4b) they were composed mostly of iron oxides, while in the case of HP they contained mixtures of oxides of iron, nickel and chromium (Fig. 4c). The Cl-rich corrosion products were present mostly in the innermost region of the scales close to or at the alloy/scale interfaces (Fig. 4b) and sometimes even within the alloy matrix (Fig. 4a). In addition, the Cr-rich Cr_7C_3 carbides of HP were preferentially attacked with respect to the matrix, forming dark regions within the alloy (Fig. 4c).

After corrosion under $ZnCl_2$-KCl deposits all the materials formed very porous scales, containing mixtures of oxides and chlorides (Figs. 5-8). The scales grown on pure Cr (not shown) contained mainly Cr_2O_3 mixed up with small amounts of chlorides, preferentially concentrated close to the alloy surface. These scales spalled off rapidly during the initial corrosion stage, leaving powder-like corrosion products on the metal surface. The scales formed on Cr-free materials such as pure Fe and CS were very thick (about

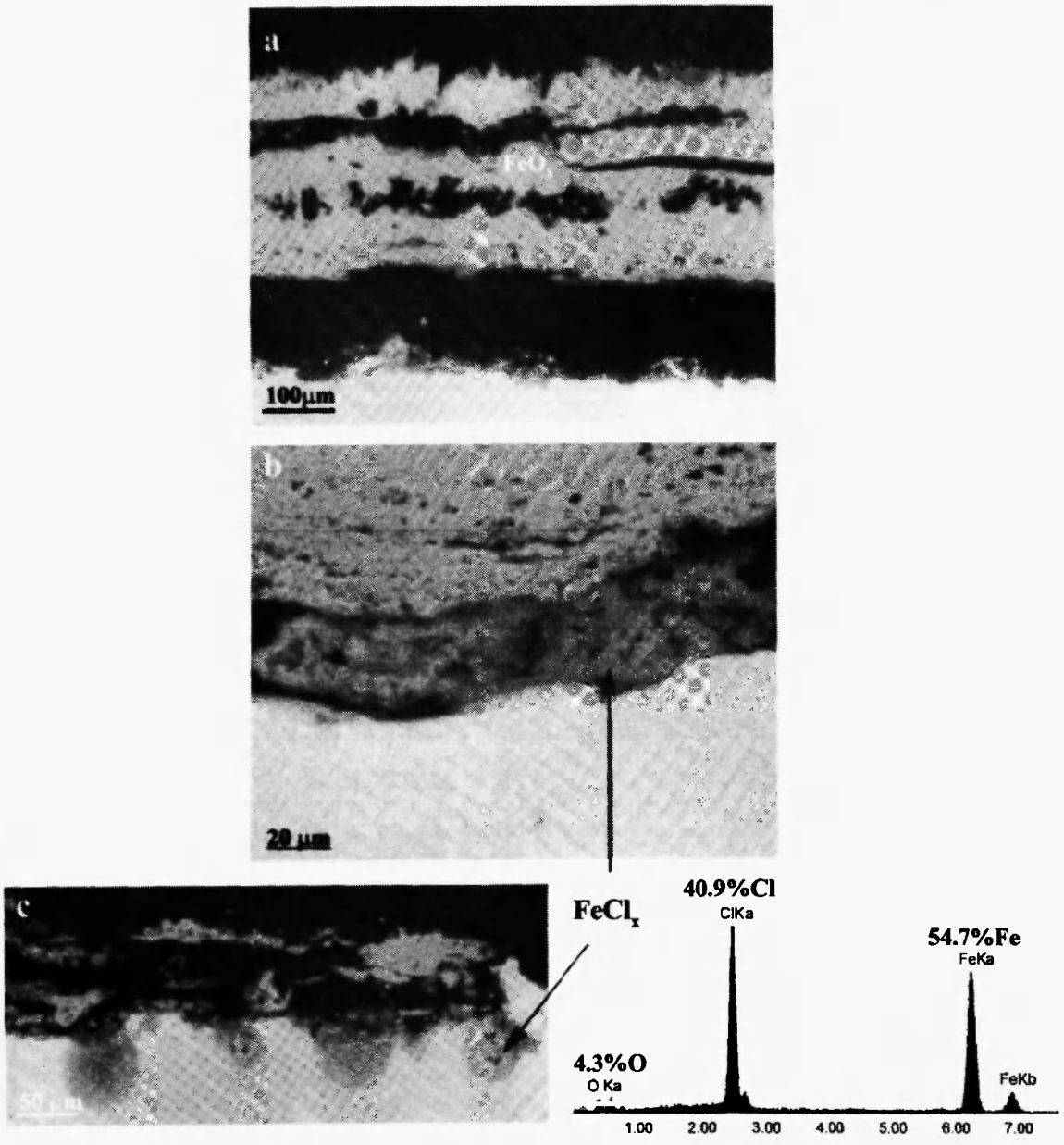

Fig. 5: Micrographs (SEM/BEI) of a cross section of a carbon steel corroded beneath a $ZnCl_2$-KCl deposit at 723K for 36 hrs. Fig. 5a: general view; Fig. 5b-c: Cl-rich compounds formed close to the alloy/scale interface.

300 μm) and exhibited a clear separation in different layers. The external scales on both materials were composed of iron oxides (Fe_2O_3 plus Fe_3O_4) plus some double Fe-Zn oxide and/or ZnO in the outermost region. A discontinuous layer rich of iron chlorides was present in the innermost region of the scale in contact with the alloy surface (Fig. 5b). In addition, a local attack in the form of pits was also present at selected locations (Fig. 5c).

The medium-Cr steel P91 and the high-Cr stainless steels SS310 corroded under the same condition also produced thick and porous external multi-layered scales of metal oxides plus a local internal formation of metal chlorides, as shown in Fig. 6 for P91 (after 35 h corrosion) and in Fig. 7 for SS310 (after only 5 h corrosion). According to the XRD and EDX examinations, the outermost layer of the external scale formed on P91 was composed of almost pure Fe_2O_3, while that grown on SS310 contained a complex mixture of Fe_2O_3 plus some NiO and ZnO. For both

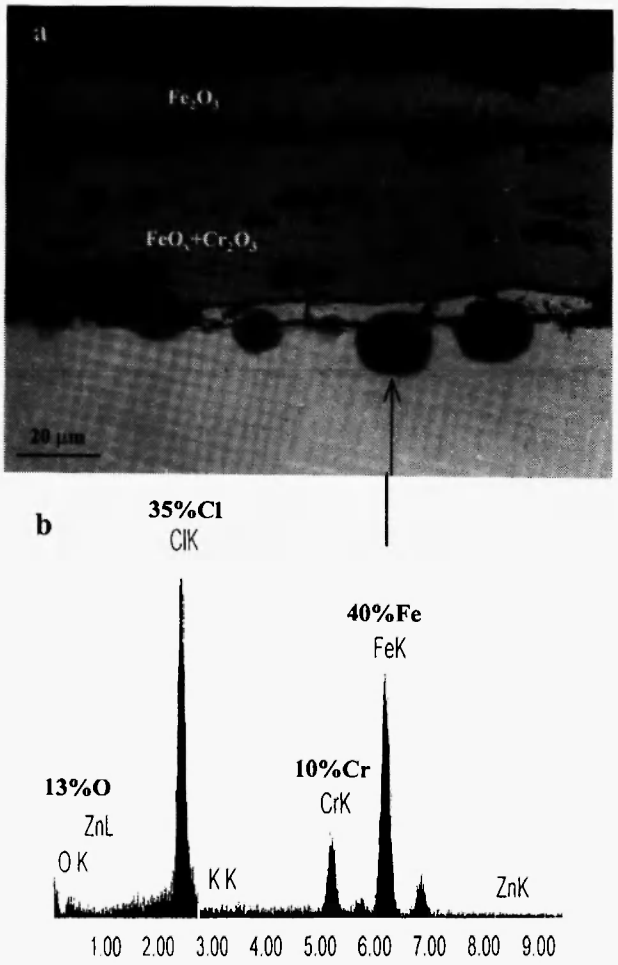

Fig. 6: Micrographs (SEM/BEI) of a cross section of a Fe-based alloy P91 corroded beneath a $ZnCl_2$-KCl deposit at 723K for 36 hrs. Fig. 6a: general view; Fig. 6b: EDX spectrum (at.%) of a Cl-rich pit in the alloy.

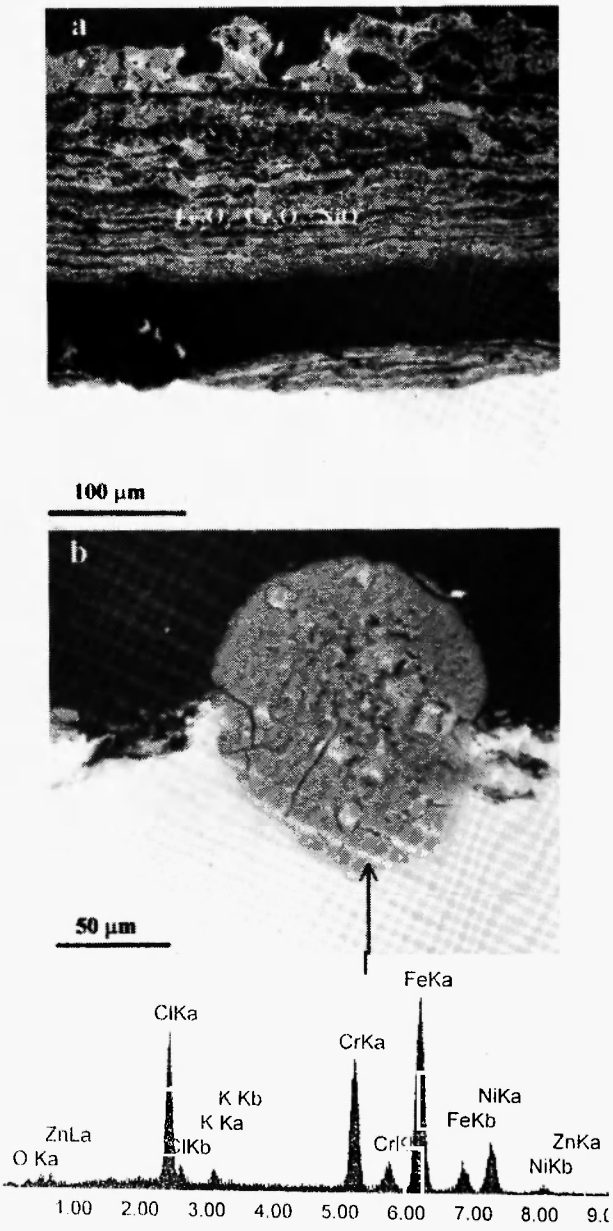

Fig. 7: Micrographs (SEM/BEI) of a cross section of SS310 corroded beneath a $ZnCl_2$-KCl deposit at 723K. Fig. 7a: general view after 5 h corrosion; Fig.7b: Cl-rich pit formed at the alloy/scale interface after 30h corrosion.

alloys, an inner layer containing a mixture of chromia and iron oxides (Fe_2O_3 plus Fe_3O_4) was also present beneath the outer Fe_2O_3 layer. Moreover, a small amount of Zn-Cr double oxide ($ZnCr_2O_4$) as well as potassium (2-3 wt%) was also found in the case of SS310. The composition of these scales was not uniform. The Cr content in the scales generally increased from the scale/salt to the scale/alloy interface. In particular, chlorine was usually enriched in the innermost scale regions at the scale/alloy interfaces or even inside the alloys (Figs. 6b and 7b), producing an irregular local internal attack. These pits were very rich in Cl and contained a mixture of chromium and iron chlorides, possibly including also some nickel chloride in the case of SS310. The EDX spectra corresponding to the local attack by chlorine in the innermost region close to the alloy/scale interfaces are presented in the corresponding figures to show the compositions of the Cl-rich compounds.

For the duplex stainless steel 2205, the external scale was again composed of mixed metal oxides with an enrichment of iron oxide (Fe_2O_3) and/or Fe-Zn double oxide ($ZnFe_2O_4$) in the outer region and of chromia in the inner region (Fig. 8a). The innermost layer of the scale (dark regions) is particularly enriched in chlorine (56.8 at.%). Moreover, an internal attack developed immediately beneath the alloy/scale interface in the form of stringers corresponding to the ferritic α phase in the original alloy, alternating with lamellae of adjacent metallic austenitic γ phase (Fig. 8b). According to the EDX analysis, the corroded areas are rich in oxygen, iron and chromium with little chlorine.

The high Cr and Ni alloy HP also formed a multi-layered external scale composed of a mixture of iron, chromium and nickel oxides (Fig. 9a). The light layers in this region corresponded to Fe-rich oxides, while the dark layers contain Cr- and/or Ni-rich oxides. An internal attack was also present, developed preferentially along the alloy grain boundaries and/or on the Cr-rich Cr_7C_3 carbides in the alloy matrix (Fig. 9b). Finally, the scale formed on the Ni-base superalloy M38G (Fig. 10) was also rather porous and composed of metal oxides rich in NiO with some Cr_2O_3 and possibly also TiO_2 and Al_2O_3. In addition, small amounts of zinc and Cl were also detected by EDX in the external scale, both more concentrated in the inner scale region, similar

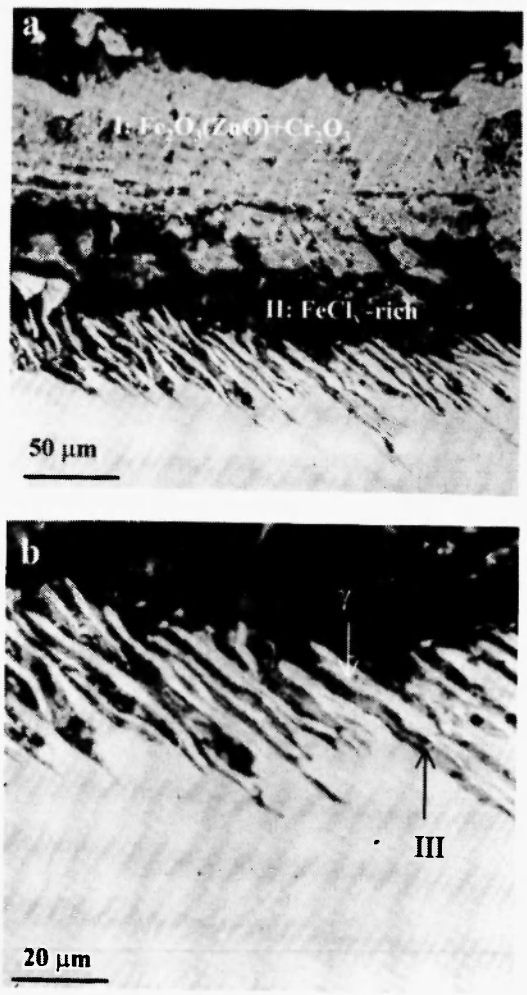

(at.%)	O	Cl	K	Cr	Fe	Ni	Zn
I	38.6	1.3	0.8	9.8	42.9	0.9	5.67
II	4.0	56.8	0.9	2.6	31.9	3.1	0.77
III	30.2	3.8	2.0	21.5	37.2	4.3	0.93

Fig. 8: Micrographs (SEM/BEI) of a cross section of the steel 2205 corroded beneath a $ZnCl_2$-KCl deposit at 723K for 29 hrs. Fig. 8a: general view; Fig. 8b: expanded view of the inner scale region.

to the behavior of the Fe-based alloys examined above. An internal attack by chlorine occurred also for this alloy (Fig. 10b).

DISCUSSION

The oxidation rates of the materials tested are quite low when they are exposed at 723K to pure oxygen

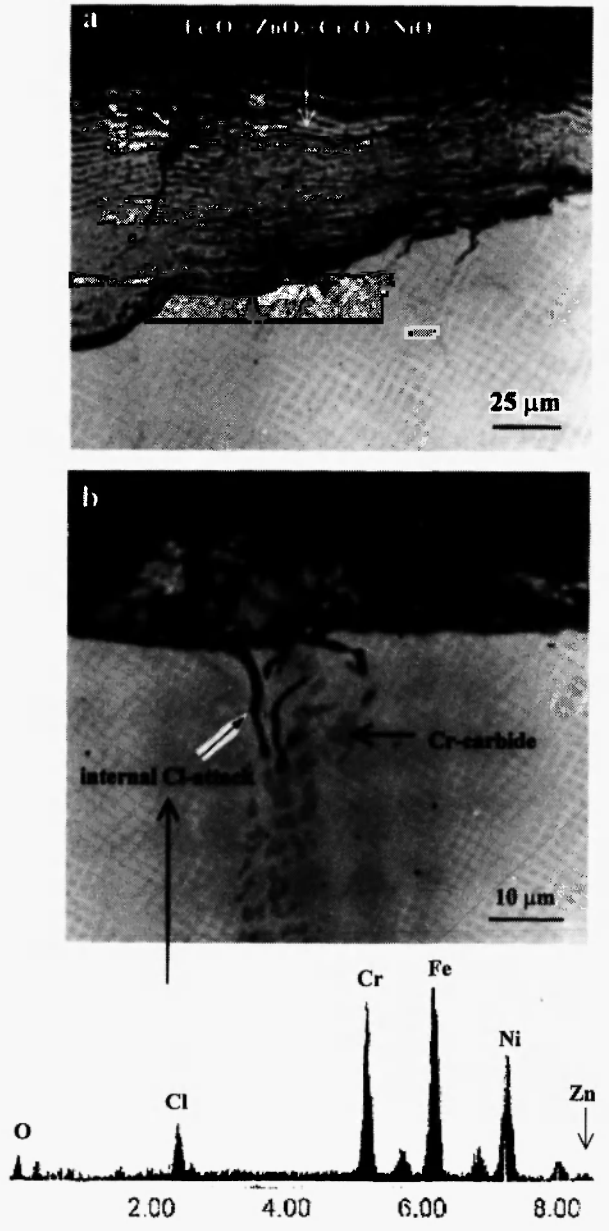

Fig. 9: Micrographs (SEM/BEI) of cross sections of the Fe-based alloy HP corroded beneath a $ZnCl_2$-KCl deposit at 723K for 5 hrs (a) and 30 hrs (b) showing internal attack along the carbides in the alloy.

without any chloride contamination, even in the absence of chlorine compounds in the gas phase. However, accelerated corrosion occurs once chlorides are present either in the molten or in the solid state. A surprising result of the present study is that higher Cr contents do not lead to an effective protection against such environments, mostly as a result of the low adherence of the corrosion products to the matrix. This behavior is quite different from the conventional hot corrosion observed in utility boilers and gas turbines where sulfates are the major components of the deposits. Similar results have also been reported previously. In particular, in a study of the hot-corrosion behavior of NaCl-coated SUS-304, SUS-316 and SUS-329J1 two-phase stainless steels, Y. Shinata found that chromium was always oxidized selectively, forming non-protective scales, so that the corrosion losses increased with increasing Cr content /6/. In these two-phase stainless steels, the ferritic phase was attacked more seriously than the austenitic phase in spite of its higher Cr content, just as observed for the corrosion of the 2205 duplex stainless steel in this study. Zahs *et al.* found that an increased Cr content of Fe-Cr alloys exposed to an $HCl/N_2/He$-5vol.% O_2 gas mixture did not induce a better corrosion resistance /7/. On the contrary, both Fe-15Cr and Fe-35Cr were covered with thick and porous scales, which were very poorly adherent to the metal/scale interface and spalled off easily. The harmful influence of Cr on the internal penetration attack on stainless steels at temperatures below the melting point of NaCl was also reported by H. Fujikawa /8/.

Thermodynamic considerations may help to gain a better understanding of the effect of Cr on the corrosion in environments containing chlorine and oxygen. The isothermal phase stability diagrams at 723K of M-O-Cl systems, where M corresponds to Fe, Cr and Ni at unit activity, respectively, are shown in Figures 11-13. Figures 11 and 12 contain also the superimposed phase diagrams for the Zn-O-Cl or K-O-Cl system at the same temperature. The phase diagrams of the Zn-Cl-O and K-Cl-O systems are not shown on the diagram for the Ni-Cl-O system since the thermodynamic data for the formation of Ni-Zn and Ni-K double oxides have not been reported so far. The relative stability of oxides and chlorides depends on the oxygen and chlorine partial pressures prevailing locally. Due to the absence of Cl_2, only oxides are stable phase in contact with the present gas atmosphere. This applies also to the chloride deposits, which in principle should gradually transform into oxides by releasing gaseous Cl_2. Alternatively, chlorine may be released by means of appropriate

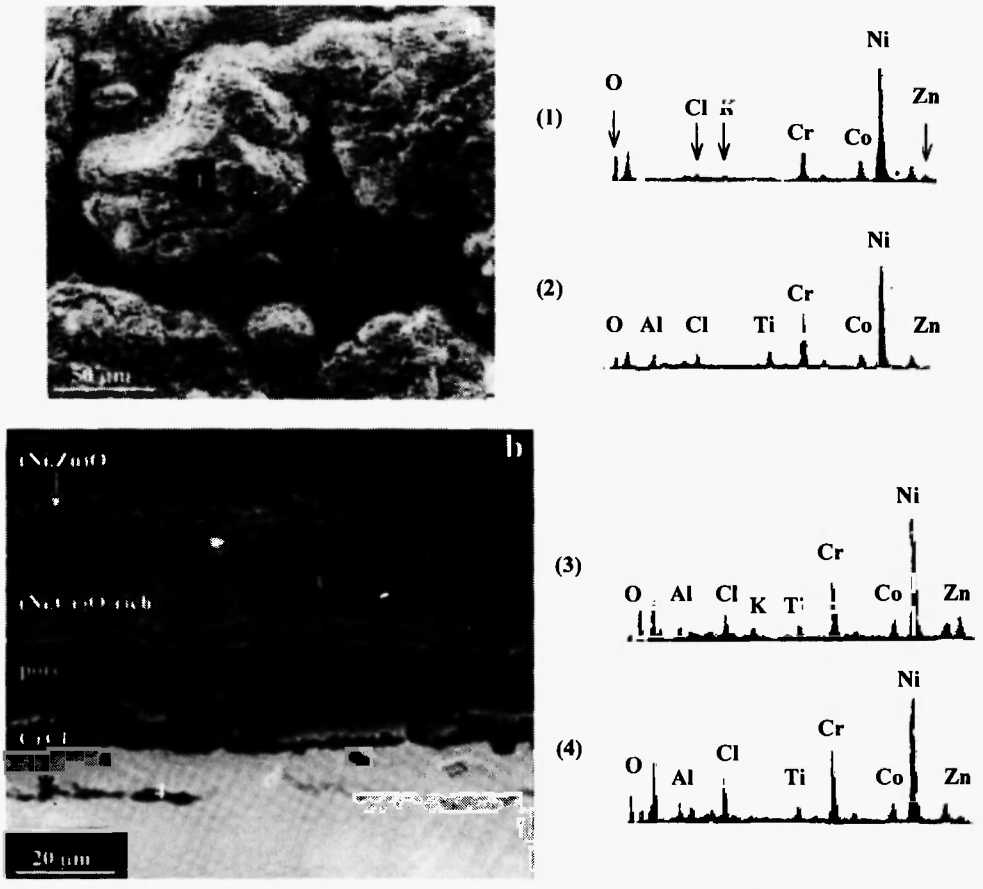

Fig. 10: Micrographs of the Ni-based alloy M38G corroded beneath a $ZnCl_2$-KCl deposit at 723K for 35 hrs with EDX spectra in different scale regions. Fig. 10a: surface morphology (SEM/SEI); Fig. 10b: cross section (SEM/BEI).

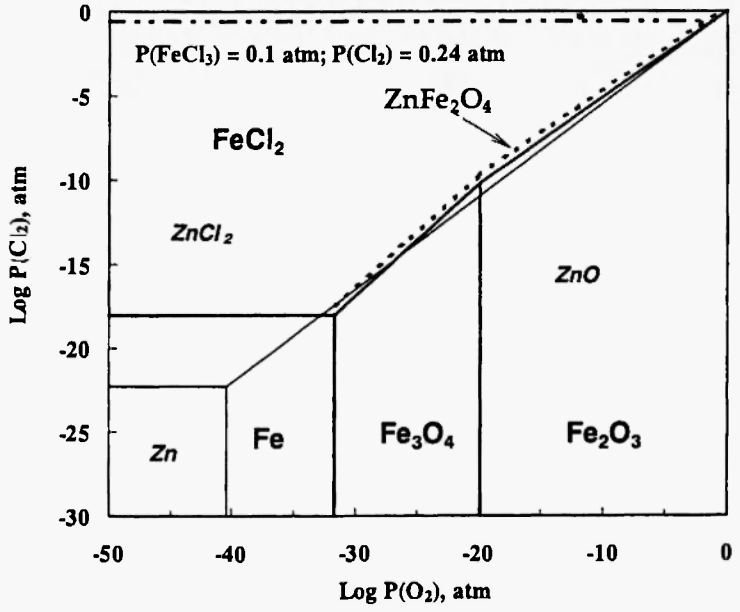

Fig. 11: Phase-stability diagrams at 723K of the ternary Fe-Cl-O plus Zn-Cl-O system with the line of equilibrium for the formation of the $ZnFe_2O_4$ double oxide.

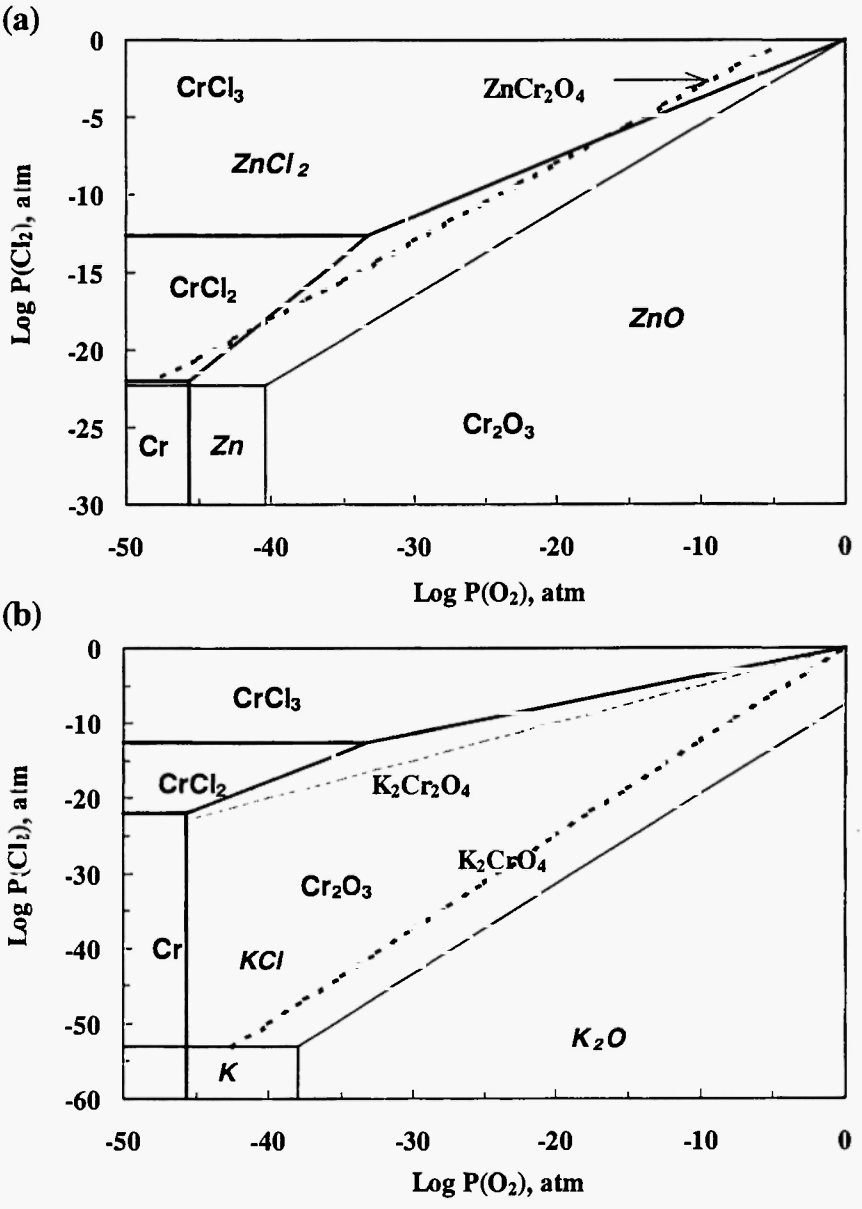

Fig. 12: Phase-stability diagrams at 723K of the ternary Cr-Cl-O plus Zn-Cl-O (a) and Cr-Cl-O plus K-Cl-O systems (b) with the lines of equilibrium for the formation of the $ZnCr_2O_4$ (a) and of the $K_2Cr_2O_4$ and K_2CrO_4 double oxides (b).

reactions between oxides in the scale and the chlorides in the deposit, which for Fe_2O_3 are:

$$2ZnCl_2+2Fe_2O_3+O_2=2ZnFe_2O_4+2Cl_2 \quad (1a)$$

$$4KCl+2Fe_2O_3+O_2=2K_2Fe_2O_4+2Cl_2 \quad (1b)$$

plus similar reactions with Fe_3O_4, while for Cr_2O_3 they are:

$$2ZnCl_2+2Cr_2O_3+O_2=2ZnCr_2O_4+2Cl_2 \quad (2a)$$

$$4KCl+2Cr_2O_3+O_2=2K_2Cr_2O_4+2Cl_2 \quad (2b)$$

or even

$$4KCl+Cr_2O_3+5/2\ O_2=2K_2CrO_4+2\ Cl_2 \quad (2c)$$

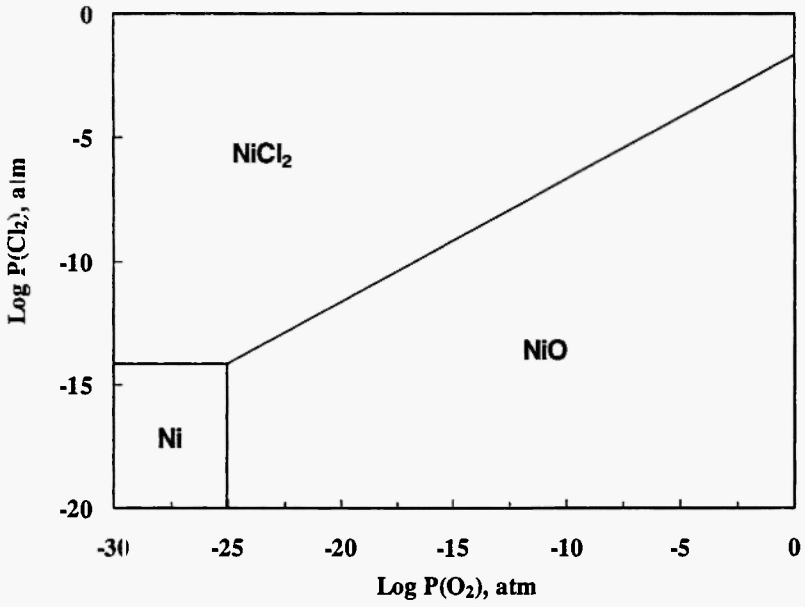

Fig. 13: Phase-stability diagram at 723K of the ternary Ni-Cl-O system.

The line marked $ZnFe_2O_4$ in Fig. 11 corresponds to the equilibrium for the reaction (1a), while those marked $ZnCr_2O_4$ in Fig. 12a and K_2CrO_4 and $K_2Cr_2O_4$ in Fig. 12b correspond to the equilibrium for the reactions (2a), (2b) and (2c), respectively. The lines for some possible additional reactions are missing because the relevant thermodynamic information is not available. Each of the previous reactions is displaced to the left (at unit activity of all the components) above the corresponding line of equilibrium, while beneath the same line the reaction is displaced to the right, producing Cl_2. Thus, in favorable cases the above reactions can occur even in regions where in their absence the oxides of the alloy components would be stable in contact with the chlorides in the deposit. This situation applies for example to reaction (2a), which may produce Cl_2 in the region intermediate between the line for the corresponding equilibrium and that for the $ZnCl_2$-ZnO equilibrium in Fig. 12a, requiring a lower oxygen pressure under a constant Cl_2 pressure or producing a larger Cl_2 pressure under a constant oxygen pressure than the reaction

$$ZnCl_2+½O_2=ZnO+Cl_2 \quad (3)$$

Thus, reaction (2a) is thermodynamically favored over reaction (3) to produce free Cl_2. The condition is somewhat similar for reaction (2c) between Cr_2O_3 and KCl to form K_2CrO_4 in Fig. 12b, while it is much more favorable for reaction 2b to form $K_2Cr_2O_4$. On the contrary, the reactions between the iron oxides and $ZnCl_2$ to form $ZnFe_2O_4$ plus Cl_2 are not favorable since the corresponding lines of equilibrium are almost overlapped with that for the $ZnCl_2$-ZnO equilibrium in Fig.11. Finally, nickel is apparently not able to form double oxides with potassium oxide, and can possibly only form a limited solid solution with ZnO, so that no line of equilibrium for double oxides has been reported in Fig. 13.

Once free Cl_2 has been generated within the oxide scale, it may then penetrate inwards as a consequence of a favorable concentration gradient, especially in the presence of porosity. Near the scale/metal interface, where the oxygen partial pressure is very low, the actual chlorine partial pressure may be sufficient to form chlorine-containing corrosion products, since the equilibrium Cl_2 pressure required locally for this reaction is also very low, making the chlorides more stable than the oxides. The chlorides of the alloy components which have quite high vapor pressures at the reaction temperature will then evaporate and diffuse outwards through the porous scale. These chlorides may then be converted again into oxides again by means of reactions such as:

$$2FeCl_3+3/2O_2=Fe_2O_3+3Cl_2 \quad (4)$$

$$2CrCl_3+3/2\ O_2=Cr_2O_3+3Cl_2 \quad (5)$$

in an outer region of the oxide scale, where the oxygen and chlorine partial pressures are favorable to this transformation. This process will produce significant growth stresses and cause the oxide scale to become less compact and protective. As a direct consequence, the transport of the various reactant species through the scale will be accelerated. This process has been termed as "active oxidation" /9/, and can also occur either in gaseous environments containing Cl species such as HCl, Cl_2 or metal chloride vapors or even beneath solid chloride films /10/.

By comparing the free energies of formation and the vapor pressures of the chlorides of the various alloy components it has been concluded that the most reactive metal among the three considered here should be Cr followed by Fe and then by Ni /11/. Moreover, a calculation of the oxygen pressures necessary for the conversion of the evaporated divalent chlorides into the corresponding oxides under a constant Cl_2 pressure by means of reactions (4) and (5) or similar shows that the Cr chloride can be converted into oxide at lower oxygen pressures than those of Fe and Ni /11/. Therefore, during their outward diffusion the evaporating Cr chlorides may be oxidized much closer to the matrix surface than those of Fe and Ni, thus producing more porosity and higher growth stresses /3,11/. This may be an important reason for the poorer adherence of the oxide scales formed on high Cr-containing materials, as shown schematically in Figure 14.

In addition to the previous reactions, a fluxing mechanism may also be involved in the corrosion induced by $ZnCl_2$ or by the $ZnCl_2$-KCl mixtures, which are molten at the reaction temperature, and be responsible for the faster degradation rate under this deposit. In fact, assuming that a low oxygen partial pressure is established at the salt/matrix interface, Fe_2O_3 may dissolve into the salt forming soluble $FeCl_3$, according to the reaction:

$$Fe_2O_3+Cl^- =2FeCl_3\ (diss.)+3O^{2-} \quad (6)$$

The dissolved Fe and the oxide-ions diffuse outwards through the molten salt to the salt/gas

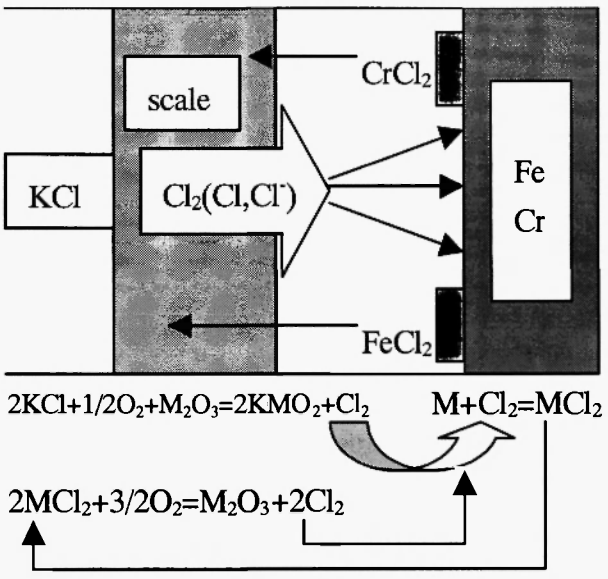

Fig. 14: Schematic presentation of the corrosion mechanism induced by chloride deposits.

interface, where Fe_2O_3 will precipitate again according to reaction (4) or to:

$$2Fe^{3+}+3O^{2-}=Fe_2O_3 \quad (7)$$

The oxide scales formed in this way are rather porous and can hardly provide any effective protection. As a direct consequence, corrosion will be significantly accelerated.

Important information concerning the dissolution of protective oxides is provided by a study of the solubility of oxide scales in molten chlorides. The solubility of Cr_2O_3 in molten NaCl-KCl mixtures has been measured at 1000K by Ishitsuka *et al.* /12/ under different partial pressures of HCl and H_2O, which control the acid-base equilibrium of molten chlorides (Fig. 15). The Cr_2O_3 films dissolved easily in the molten chlorides mixture forming hexavalent Cr ions according to the reaction:

$$Cr_2O_3+3O_2+4O^{2-}=4CrO_4^{2-} \quad (8)$$

and thus lost their protective properties /12/. Furthermore, on the basis of the phase stability diagram for the Na-Cr-Cl-O system at 623K, Otsuka showed that the dissolution of protective Cr_2O_3 scales by acidic fluxing might result in the formation of the highly

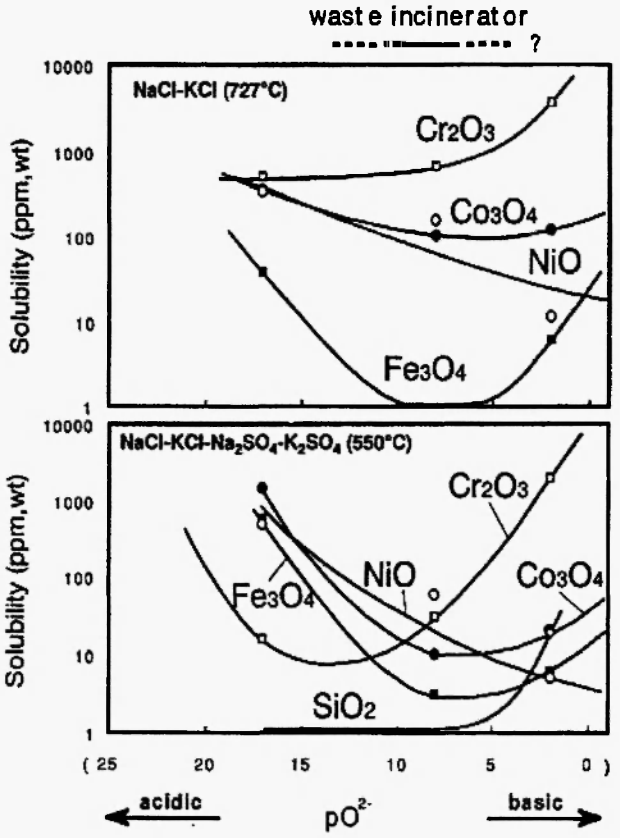

Fig. 15: Solubility of various metal oxides in molten chlorides /12/.

volatile species CrO_2Cl_2 /13/, which may explain the occurrence of a self-sustaining, accelerated hot corrosion for Cr_2O_3-forming steels. Since the oxide scales formed beneath the KCl-$ZnCl_2$ mixed deposit used in the present study are always rather porous and can hardly provide any effective protection, the oxygen supply could be more than sufficient for the above reaction to occur.

Finally, the chlorides can also produce a strong internal attack, especially for steels containing Cr-rich carbide precipitates. In fact, fully over-sensitized steels tend to suffer from more severe inter-granular attack than solution-treated steels due to the preferential attack of Cr carbides by chlorine. In the present study, a preferential attack of the Cr_7C_3 carbides, which may be described by the reaction:

$$2Cr_7C_3+14Cl_2+3O_2=14CrCl_2+6CO \quad (9)$$

was clearly present in the corrosion of HP (Fig. 9b). Therefore, besides having a deleterious effect on the general corrosion of steels, Cr may also exhibit a harmful influence on the strength of internal attack.

CONCLUSIONS

The corrosion behavior of pure Fe and Cr and of several Fe-based alloys with different Cr contents, was examined at 723K in the presence of chloride deposits in 0.1MPa pure oxygen. In spite of the absence of chlorine compounds in the gas phase, all of the materials examined suffered from accelerated corrosion, characterized by the formation of porous oxide scales which spalled off readily from the matrix, while the adherence of the corrosion products to the substrate was inferior in high Cr-containing materials. Chlorine was enriched at the scale/substrate interface and also induced local corrosion internally to the matrix, as evidenced by the preferential attack of the Cr_7C_3 carbides in the HP steel and of the Cr-rich phase in the 2205 duplex steel.

ACKNOWLEDGEMENT

Partial financial support by the NSFC (China) under the research contract No. 59725101 is gratefully acknowledged.

REFERENCES

1. Y.S. Li, Y. Niu and W.T. Wu, *Corrosion Science and Protection Technology* (in Chinese), **12**, 224 (2000).
2. E. Otero, A. Pardo, F.J. Perez, M.V. Utrilla and T. Levi, *Oxid Met.*, **49**, 467 (1998).
3. Y.S. Li, Y. Niu and W.T. Wu, *CORRORION/2001, Paper No. 01158.* (Houston, TX: NACE International, 2001).
4. M. Spiegel. *Mater Corros.*, **50**, 373 (1999).
5. Y.S. Li, Y. Niu and W.T. Wu. *Rare Metallic Material and Engineering* (in Chinese), **30**, 376 (2001).
6. Y. Shinata, F. Takahashi and K. Hashiura, *Mater Sci Eng,*. **A87**, 399 (1987).

7. A. Zaha, M.Spiegel and H.J.Grabke, *Mater Corros.*, **50**, 561 (1999).
8. H. Fujikawa and N. Maruyama. *Mater Sci Eng,*. **A120**, 301 (1989).
9. Y. Y. Lee and M.J. McNallan, *Metallurg. Trans.*, **18A**, 1099 (1987).
10. Y.S. Li, Y. Niu and W.T. Wu, *Corros Sci & Protect Technol* (in Chinese), **12**, 41 (2000).
11. A. Zahs, M. Spiegel and H.J. Grabke, *Corros Sci.*, **42**, 1193 (2000).
12. T. Ishitsuka and K. Nose, *Mater Corros,*. **51**, 177 (2000).
13. N. Otsuka, T. Kudo, in: *High Temperature Corrosion of Advanced Materials and Protective Coatings,* Y. Saito, B. Onay and T. Maruyama (Eds.), North Holland: Elsevier Science Publishers, 1992; pp.205-211